Korean J. Chem. Eng., **28**(6), 1372-1379 (2011)
DOI: 10.1007/s11814-010-0522-y

Experimental and computational fluid dynamics modeling of mixing by Visco-jet impellers

Masoud Rahimi*,†, Saeideh Amraei*, and Ammar Abdulaziz Alsairafi**

*CFD Research Center, Chemical Engineering Department, Razi University, Kermanshah, Iran
**Faculty of Mechanical Engineering, College of Engineering and Petroleum, Kuwait University, Kuwait
(*Received 22 October 2010 • accepted 17 December 2010*)

Abstract−This paper reports experimental and computational frluid dynamics (CFD) studies on an impeller called Visco-jet with the aim of finding the effect of two side diameters ratio of its blade, which has a semi-conical shape, on drawdown process of floating polymericparticles into high viscosity glycerin solution. Nine different geometries were examined experimentally, and there were significant differences in their performance. The results reveal that when diameter of smaller side of semi-cone impeller is half of the other side, mixing was performed in a more efficient way. The CFD-predicted results have been used for explaining the experimental observation. The CFD-predicted hydrodynamics parameters confirm superiority of this geometry compared with the other ones.

Key words: CFD, Visco-jet, Mixing, Modeling Viscous Fluid

INTRODUCTION

Food processing, polymerization reactions, fermentation processes, wastewater treatment and minerals processing are some examples of industrial processes during which the drawdown of floating solids is required [1,2]. Due to the wide range of applications, the process requirements (whether just draw down, homogeneous dispersion or dissolution) can be quite different. Particle properties (whether floating because of density difference, or poor wet ability, or low apparent bulk density, etc.)as well as hydrodynamic effects (such as the impeller speed, diameter, position, power input, etc.) are the key factors affecting the performance of these processes. Despite of the vast amount of research done on the suspension of heavy solids from the vessel base, there are limited published works on the drawdown of floating solids from the liquid surface [3].

In many cases successful suspension of solids has a significant influence on the quality and/or quantity of the final products. In most industrial solid/liquid mixing, systems involve suspension of solids particles which are heavier than the liquid, and these suspensions have received extensive research attention. On the other hand, there are several applications where solids are lighter than the liquid and require a pulling down action to produce homogeneous slurries. The suspension of floating solids is of particular interest in minerals processing, fermentation and sewage treatment [4].

The complete drawdown of floating solids by agitated liquids in stirred tanks can be achieved in two different ways. In full-baffled tanks, where the formation of the vortex is suppressed by the presence of the baffles, the intensity of turbulence is primarily responsible for particle dispersion. In this case, energy dissipation and the position of the impeller with respect to the liquid surface were found to be the controlling parameters. When alternative baffle configurations were used instead, it was found that the liquid swirl in tanks provides a mechanism for pulling down of the floating particles into the bulk [4].

Mixing of highly viscous fluids is mainly carried out in the laminar regime. It is often associated with poor bulk mixing, an inhomogeneous distribution of the various phases, and presence of rheological complexitiessuch as shear thinning or thickening behavior. In the laminar regime, mixing is obtained by a stretching-folding-breaking mechanism of the secondary phase and not by highly energetic eddies in the turbulent regime, which makes the design of the mixer a challenging task [5].

Various impellers have been proposed to respond to needs for laminar viscous mixing. They are based either on an enlargement of open impellers (wider blades with large diameters) or close-clearance designs such as anchors and helical ribbons [6].

The Visco-jet impeller is a new impeller that has recently gained more attention. The Visco-jet mixing system is the result of the so-called cone-principle. The Visco-jet homogenizes low and high viscosity liquids in vessels by creating dynamic flow conditions. This impeller has been employed in beverage production, dairy production, food, sugar and candy production, water treatment, cosmetics, colorant/paint production, paper manufacture, etc. Despite this huge number of applications, few studies have been published about its mixingcharacteristic and performance.

In recent years, the numerical modeling of mixing in a stirred tank (reactor) has attracted a great deal of attention [7]. The developments in computational fluid dynamics (CFD) have accelerated in the past two decades due to the spectacular progress in digital computing. The CFD modeling may not completely eliminate the necessity for experiments, but it can synergistically guide the experiments and our understanding from process hydrodynamics [8,9].

The general practice for the evaluation of stirred vessels has been done over the years through the experimental investigation for a number of different impellers, vessel geometries, and fluid rheology. Such an approach is usually costly and sometimes is not an easy task. Using CFD, it is possible to examine various parameters con-

†To whom correspondence should be addressed.
E-mail: masoudrahimi@yahoo.com

tributing in the process in a shorter time and with a less expense, tasks which are quite expensive in experimental examination. The capability of CFD to forecast the mixing behavior in terms of mixing time, power consumption, fluid flow pattern and velocity profiles is considered a successful achievement of this type of modeling [10].

Kasata et al. [11] have presented a computational approach to simulate solid suspension in a stirred reactor for a wide range of operating conditions. A similar approach was used to simulate the solid-liquid flows generated by the Rushton turbine. The model predictions were compared with the experimental data of axial solid concentration profile reported by Yamazaki et al. [12]. The model predictions were used to understand the interaction of the suspension quality and the liquid-phase mixing process.

Barailler et al. [13] studied the characterization of the hydrodynamics of a rotor-stator mixing in the laminar regime with viscous Newtonian fluids. They found that the numerical prediction of the power consumption and flow profiles is in good agreement with their experimental data.

The drawdown of floating solids from the liquid surface has been investigated using vessels of 0.61 and 2.67 m diameter by Taskin [14]. The importance of impeller type (mixed flow pitched blade turbine (PBT) and the narrow blade hydrofoil LE-20), pumping mode and position and the effect of varying liquid height were studied.

Taskin and Wei [3] investigated the effect of impeller-to-tank diameter ratio (D/T) on the drawdown of solids using a mixed flow impeller (pitched blade turbine) and a narrow blade hydrofoil (LE-20 (APV (now HaywardTyler Fluid Handling Limited) proprietary impeller)) of D=T/2 and T/3. Operational conditions (impeller speed and power consumption) at which solids do not remain at the liquid surface for more than 2-4 s were determined for a given solid type polyethylene particles) at a given concentration (X=1%). Under selected conditions, liquid velocity values were obtained using LDA measurements and CFD modeling in order to better interpret the findings.

Westhuizen et al. [15] investigated the solids suspension in a pilot-scale mechanical flotation cell in terms of the critical impeller speed (Njs), whichrepresented the effectiveness of solid suspension in stirred tanks. They determined critical impeller speeds and measured the concentration profiles through sample withdrawal pilot flotation cell. They studied the critical impeller speedfor describing the effectiveness of solids suspension in a mechanical flotation cell. The authors speculate that, when solids suspension is considered as a precondition to flotation, flotation cells should not be operated at specific 'impeller speeds' but rather at specific 'percentages of critical impeller speed' analogous to the 'critical speed' used in the operation of grinding mills.

With regard to the above-mentioned studies, in the present work it has been tried to illustrate the effect of geometry of a Visco-jet impeller on mixing performance. In other words, the effect of small to large diameter ratio of cones of a Visco-jet impeller on the draw down of floating particle has been investigated. In this research, the CFD modeling and experimental works were performed in a high viscosity medium for unbaffled configuration. The main objective of the present work is to select a more efficient geometry for the Visco-jet impeller. The hydrodynamic parameters such as power consumption, power number, local axial flow number, average axial flow number and axial circulation time have been calculated for all the sizes of impellers. In addition, the speeds of just draw down (N_{JD}) for all studied sizes have been calculated and compared.

EXPERIMENTAL WORK

The stirred vessel inthe experiments is a cylindrical, flat-bottomed tank with a diameter of T=0.14 m. The height of the liquid (H) has been selected to be 0.14 m, which is equal to the tank diameter. The tank equipped with four vertical baffles mounted on the wall, with a width of T/12. Agitation is provided by a Visco-jet impeller with a diameter of D=T/2 and placed on a 0.01 m diameter for shaft. The bottom impeller clearance, C, was set to be equal to the impeller diameter. Table 1 gives the dimensions of the tank and its geometrical characteristics. The impeller power consumption and speed were measured using a rotary-torque transducer with an encoder disk. A schematic view from the experimental rig is shown in Fig. 1.

In the present study various Visco-jet impellers with different small cone sizes and the same large cone size were fabricated. Fig. 2 shows different views of all fabricated impellers with different small to large cone ratios.

The experiments were carried out for unbaffled configuration the liquid phase was glycerin solution and the solid phase was poly-

Table 1. Summary of the geometrical configurations of studied mixing tank

Vessel diameter, T(m)	0.14
Liquid height, H(m)	0.14
Liquid volume, V(m^3)	$0.21*10^{-2}$
Impeller diameter D(m)	0.07
Shaft diameter (m)	0.01

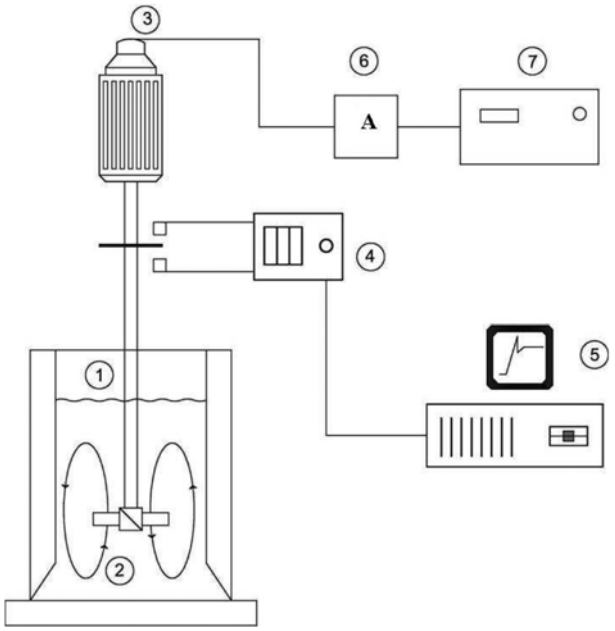

Fig. 1. Experimental set-up.

1. Tank
2. Impeller
3. Electromotor
4. Optical tachometer
5. Computer
6. Aampermeter
7. Power generator

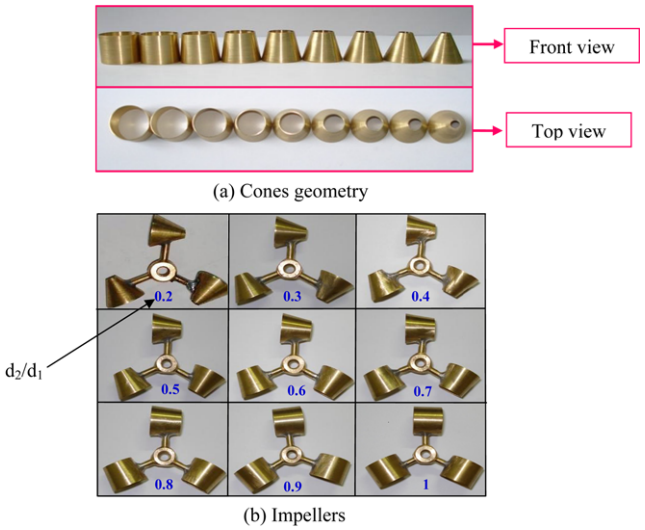

Fig. 2. The impeller geometry at various small to large cone diameters.

meric particle. The solid particles have a density of 1,000 $kg \cdot m^{-3}$ which is lower than that of glycerin solution.

In the field of particle mixing in a liquid, some research was focused on the motion of particles at the liquid surface and some other studies based their judgments on the incorporationof solids into the liquid phase for certain periods of time [3,16]. Here, conditions over which particles drawdown from the free surface were determined from mixing visualization test. For most industrial applications, minimum solid motion at the surface is not sufficient and particle drawdown into the liquid is demanded. In the present research, the impeller rotation speed in which no particles remain floating on the liquid surface for more than 4-6 s ($N_{JD4\text{-}6}$) has been used as a criterion for efficientmixing. The $N_{JD4\text{-}6}$ for various types of impellers have been found for unbaffled examined stirred tank. In addition, primary or minimum rotation speed ($N_{JD(f)}$) of impeller that the first particles were drawn down from the free surface was determined.

Fig. 3. illustrates the measured rotational speed of $N_{JD(f)}$ and $N_{JD\ 4\text{-}6}$ for all employed impellers. The reported values are averages of three times measurements of these parameters with maximum uncertainty of ±3%. Fig. 3(a) shows the effect of diameter ratio on N_{JD}. The results reveal that the first particle drawdown inside the liquid in an impeller speed of 132 rpm as the impeller with a size ratio of d_2/d_1=0.5 was employed. However, this speed is 165 rpm for cylindrical shape impeller (d_2/d_1=1). In Fig. 3(b) the impeller rotation speed that particles remain at the liquid surface for 4-6 s is illustrated. This figure shows that more efficient mixing was established by the optimum size impeller ratio of d_2/d_1=0.5. However, the results show that the worst impeller size is d_2/d_1=0.2, which needs an impeller speed of 265 rpm to establish particles remaining at the liquid surface for 4-6 s.

On the other hand, Fig. 4 shows power consumption by the different examined impeller to distribute the particles into liquid. The

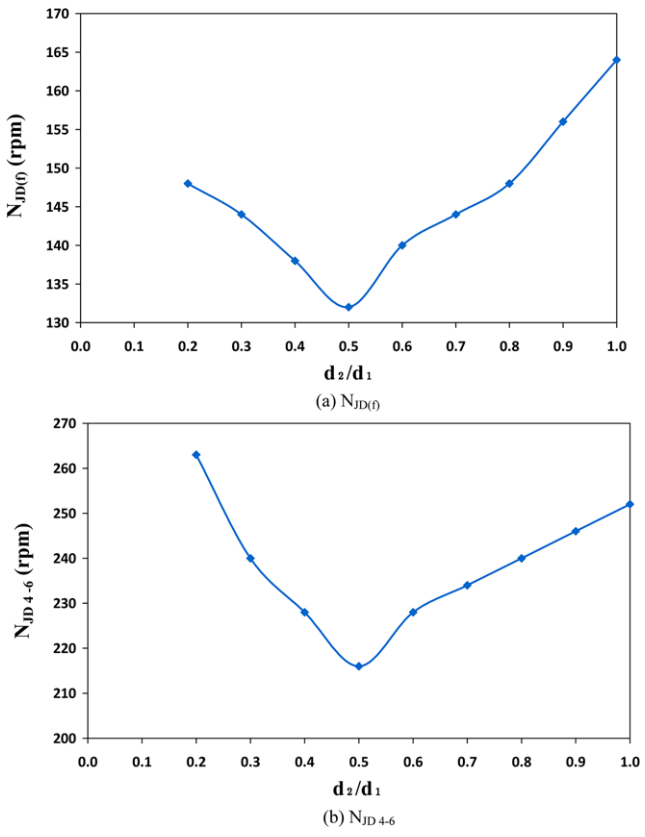

Fig. 3. Effect of different geometries of impeller on drawdown speed (±3%).

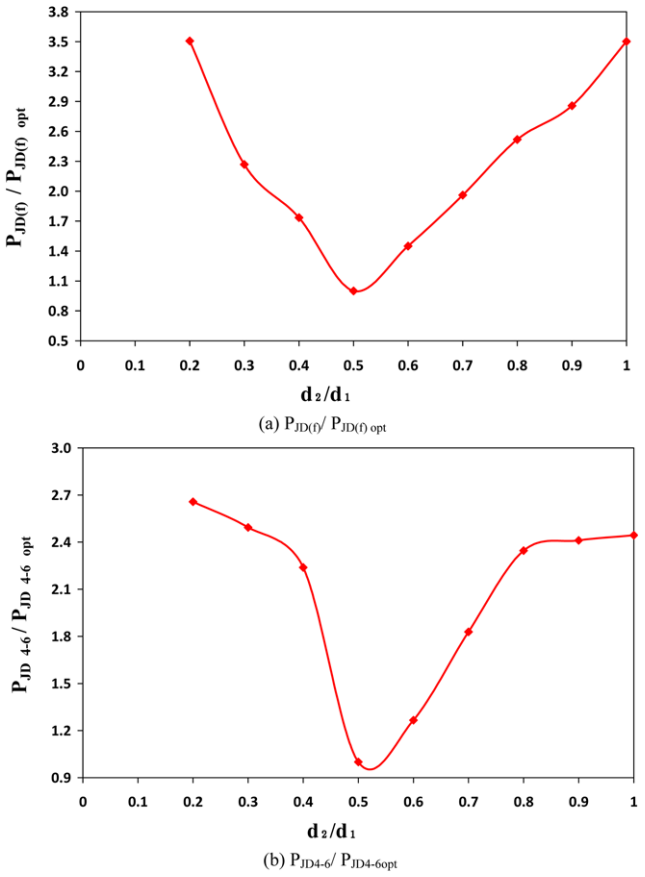

Fig. 4. Ratio P/ Popt(±5%)for different impeller geometries.

reported values are averages of three times measurements of these parameterswith maximum uncertainty of ±5%. The figure represents the ratio of power consumption by different impellers with respect to the efficient one (d_2/d_1=0.5), which used the lowest power. Fig. 4(a) represents the power consumption by impellers to draw-down the first particle. The results show that the impeller with the lowest and highest ratio of d_2/d_1 used more power. This ratio is 3.5 times of the efficient one for d_2/d_1=0.2. Fig. 4(b) represents the power consumption ratio for $P_{JD4\text{-}6}$. The results show that the impeller with d_2/d_1=0.2 used 2.7 times of power needed for d_2/d_1=0.5 to establish the same quality of fluid/ particle mixing.

NUMERICAL WORKS

1. Theory

The fluid dynamic and particle motion are modeled using a 3-D CFD model by employing the discrete particle method (DPM) approach for solid suspension. In modeling, the SIMPLE method to integrate the volume-averaged Navier-Stokes equation and the DPM is based in the Newton equation of particle motion [16].

Similar to the gas-solid system, the liquid-solid fluidization is usually studied using a continuum approach that views the liquid and solid phase as two interpenetrating media, each phase governed by conservation laws, either postulated or derived by averaging local properties (void fraction, pressure, fluid velocity) of the fluidized bed [17].

The main reason for using of the DPM model in this work is the flexibility offered in studying the dynamics of the fluidized system. The simulation approach adopted in this research is a hybrid of CFD and the DPM. The CFD modeling was used to consider the fluid phase and DPM for tracking particle motion [16].

The generalized set of governing equationsfor liquid-solid fluidization systems at constant temperature can be listedas follows: [16-19]

Continuity equations:

Fluid phase:

$$\frac{\partial \varepsilon\rho_f}{\partial t}+\nabla\cdot(\varepsilon\rho_f u)=0 \tag{1}$$

$$\frac{\partial (1-\varepsilon)\rho_s}{\partial t}+\nabla\cdot(1-\varepsilon)\rho_s v=0 \tag{2}$$

Momentum equation:

Fluid phase:

$$\frac{\partial(\varepsilon\rho_f u)}{\partial t}+\nabla\cdot(\varepsilon\rho_f uu)=-\varepsilon\nabla p-\beta(u-v)+\left[\nabla\cdot\varepsilon\left\{-\frac{2}{3}\mu_f(\nabla\cdot u)E\right\}\right]+(\nabla\cdot\varepsilon\{\mu_f[\nabla u+(\nabla u)^T]\})+\varepsilon\rho_f \tag{3}$$

Solid phase:

$$\frac{\partial[(1-\varepsilon)\rho_s v]}{\partial t}+[\nabla\cdot(1-\varepsilon)\rho_s vv]=-(1-\varepsilon)\nabla p+\beta(u-v)+\left[\nabla\cdot\left(1-\varepsilon\left\{-\frac{2}{3}\mu_s(\nabla\cdot v)E\right\}\right)\right]+(\nabla\cdot(1-\varepsilon)\{\mu_s[\nabla v+\nabla v^T]\})-G(\varepsilon)\nabla\varepsilon+(1-\varepsilon)\rho_s g \tag{4}$$

Constitutive equations:

Fluid-solid momentum transfer coefficient:

$$\text{For } \varepsilon\le 0.8:\ \beta=150\frac{(1-\varepsilon)^2}{\varepsilon^3}\frac{\mu_f}{(\Phi_s d_p)^2}+1.75\frac{(1-\varepsilon)}{\varepsilon^3}\frac{\rho_f}{\Phi_s d_p}|u-v| \tag{5}$$

$$\text{For } \varepsilon>0.8:\ \beta=\frac{3}{4}C_d\frac{\varepsilon(1-\varepsilon)}{\Phi_s d_p}\rho_f|u-v|\varepsilon^{-2.65} \tag{6}$$

Where:

$$C_d=\frac{24}{Re_p}[1+0.15(Re_p)^{0.687}];\ Re_p<1000 \tag{7}$$

$$C_d=0.44;\ Re_p\ge 1000 \tag{8}$$

and

$$Re_p=\frac{\varepsilon\rho|u-v|d_p}{\mu_f} \tag{9}$$

2. CFD-DPM Model

Unlike the two-fluid model, the CFD and DPM (CFD-DPM) approach establishes a set of Navier Stokes equations for the liquid phase and the Newtonequation of motion for each particle of the discrete solid phase. The most common assumptions in simplifying the transport equations for liquid-solid fluidization process are isothermal conditions, incompressible fluid (constant density), and constant viscosity. The Eulerian-Lagrangian model is a synonym of the CFD-DPM model. Some commercial CFD software uses this approach in their framework of fluid-droplet simulation [16].

In the Eulerian-Lagrangian approach, the motion of the continuous phase is modeled using a conventional Eulerian framework, while the trajectories of the dispersed phase particle are simulated by solving an equation of motion for each dispersed particle. Particle acceleration in Cartesian coordinates can be written as [16,17]:

$$\frac{du_i^p}{dt}=F_D(u_i-u_i^p)+g_i(\rho_p-\rho)/\rho_p+F_i/\rho_p \tag{10}$$

Here u_i and $u_{i,p}$ are the fluid and particle velocity in the i-direction, respectively. Other variables are g_i, acceleration of gravity in the i-direction, ρ_p, particle density, ρ_l, fluid density [16,17].

The term F_D, in the above equation can be written as:

$$F_D=\frac{18\mu C_D Re}{\rho_p d_p^2\ 24} \tag{11}$$

Where μ is the viscosity of the fluid, ρ_p is the density of the bubble and d_p is diameter. Re stands for the relative Reynolds number, which is defined as:

$$Re=\frac{\rho_l d_p|u_p-u_l|}{\mu} \tag{12}$$

Eq. (10) incorporates additional forces (F_i) in the particle force balance that can be important under special circumstances. This additional force includes virtual mass, thermophoretic, Safman's lift force, forces in rotating reference frames and Brownian forces [16,17].

3. CFD Modeling

To study the mixing process, the commercial FLUENT™ was used to model the steady-state 3D flow field generated by Visco-jet impellers. A pre-processor (GAMBIT™) was used to discretize the

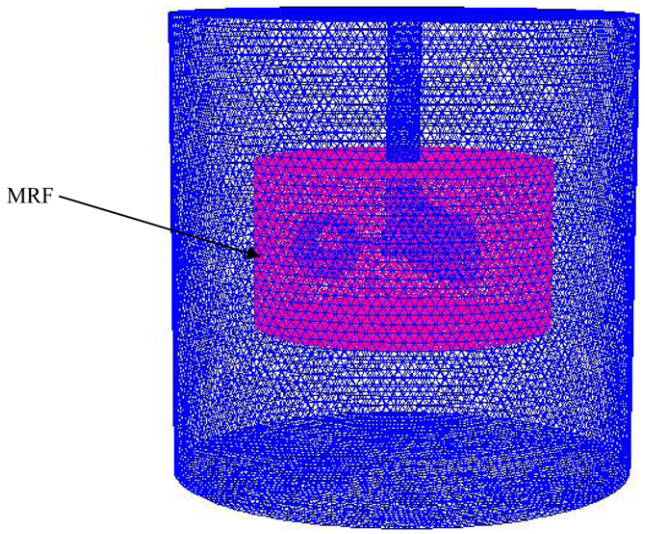

Fig. 5. Mashed tank and MRF section.

flow domain with a tetrahedral mesh. The mixing tank was meshed into 832416 control volumes. In general, the density of cells in a computational grid needs to be fine enough to capture the flow details, but not too fine, since problems described by large numbers of cells require more CPU time to solve. This number of control volume was found after a grid independency check. To capture the boundary layer flow detail, a higher mesh density was used near the tank wall and the rotating impeller [16].

In the present work, the rotating frame of reference (MRF) technique was used to model impeller rotation. The MRFwas used for the region containing the impeller,while a stationary frame was used for regions that are stationary containing the tank walls. Fig. 5 reveals the mesh configuration as well as the MRF section in studied tank.

3-1. Solution Strategy

The analysis has been carried out in two steps. Firstly, the velocity and pressure fields in the tank were solved. These values were then used to calculate particle trajectories with the flow field. The SIMPLE pressure-velocity coupling algorithms, standard pressure, second-order upwind discretization scheme for momentum were employed in the modeling [16,17]. Simulations were considered converged when the scaled residuals for each transport equation were below 1×10^{-5}. Most models required about 5,000-6,000 iterations for convergence.

The DPM was used to model the particle movement and drawdown of particles in the fluid. As the particle volume percent was less than 10%, therefore, the presenceof particles does not have any effect on predicted fluid flow pattern and velocities [16]. In the modeling, the number of particle streams, injection type and particle type were set at 400, surface and inert, respectively.

FLOW CHARACTERIZATION TOOLS AND METHODS

Two main groups of analysis techniques were used in this work in order to judge solid-liquid mixing quality. The first group concerns macroindicators such as power number, circulation number, impeller flow number and axial flow number. The second group presents local indicators such as velocity profiles, streamlines and particles tracking. Statistical methods such as probability density function of stretching [20] were not used in this work.

1. Power

The interest of power calculation is to evaluate energy consumption and its economic impact. Power consumption used for mixing, P, can be calculated by various methods. One of these methods uses the torque, C, applied on the agitation system as given in Eq. (13). With this method, the power can be calculated for each impeller using the following equation:

$$P=2\pi NC \tag{13}$$

In which N is the impeller rotational speed.

In mixing, the flow regime is characterized by the Reynolds number, Re, defined in agitated tank as [20]:

$$Re=\frac{\rho ND^2}{\mu} \tag{14}$$

Where D is the impeller diameter (in m) and N is the rotational speed (rpm) where ρ is the liquid density (kg m^{-3}).

2. Axial Flow Number and Average Axial Circulation Time

An axial flow number is defined for it to characterize well enough the loops connection. The axial flow rate, Q_{ax}, at different heights in the vessel is evaluated by the surface integration of either the positive, v_{+z}, or negative, v_{-z}, component of the axial velocity at particular horizontal plane: [20]

$$Q_{ax}(z)=\int_A v_z^+ dz=\int_A v_z^- dz \tag{15}$$

Where A is the radial section of the tank.

The average axial flow rate, Q_{Aax}, for the entire vessel is defined as: [20]

$$Q_{Aax}=\frac{\int_0^H Q_{ax}(z)dz}{\int_0^H dz} \tag{16}$$

Both the axial flow rate and the average axial flow rate can be normalized by ND^3 to give the dimensionless axial flow number, $N_{Q_{ax}}$, and the dimensionless average axial flow number, $N_{Q_{Aax}}$, respectively:

$$N_{Q_{ax}}(z)=\frac{Q_{ax}(z)}{ND^3} \tag{17}$$

$$N_{Q_{Aax}}=\frac{Q_{Aax}}{ND^3} \tag{18}$$

Finally, the average axial circulation time, t_{ax} can be defined as follows [20]:

$$t_{ax}=\frac{V}{Q_{Aax}} \tag{19}$$

RESULT AND DISCUSSION

1. Predicted Flow Pattern

The 3-D CFD analysis has been used to explain the experimental observations. In the first stage the predicted flow pattern estab-

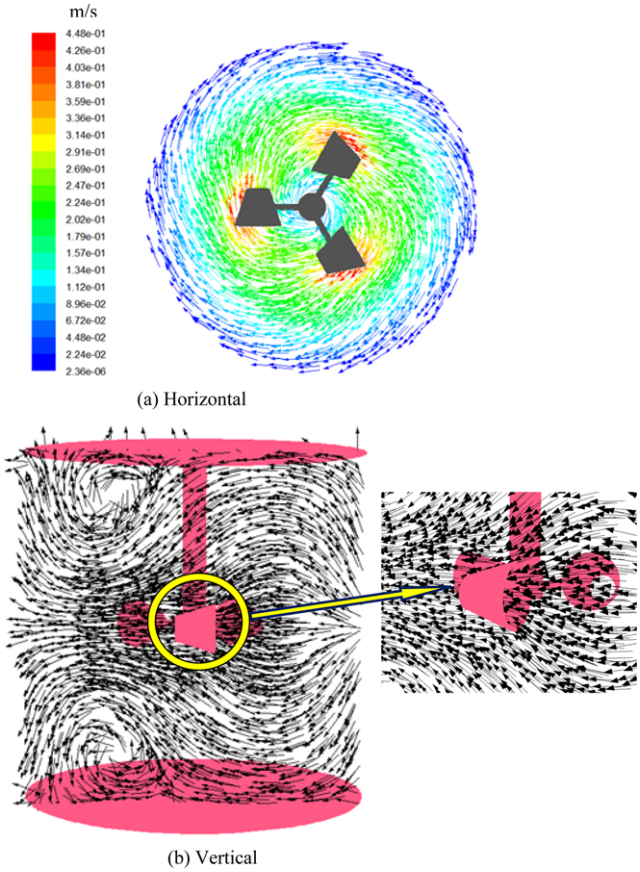

Fig. 6. Predicted fluid flow pattern (d_1/d_2=0.5).

lished by this type of impeller is shown in Fig. 6. The d_2/d_1=0.5 size ratio is used for this purpose. The velocity vectors in vertical and horizontal slices are illustrated in this figure. Thehorizontal slice in the impeller level reveals a tangential flow pattern induced by the impeller. On the other hand, the vertical slice, which goes through one of impeller's blade (semi-cone), illustrates how fluid moves axially. Moreover, the way that fluid enters from wider side of the blade and exits from the jet side is illustrated.

In Fig. 7(a) qualitative comparison between experimental observation and CFD predicted paths traveled by the particles is presented. This figure relates to the way that the particle drawdown

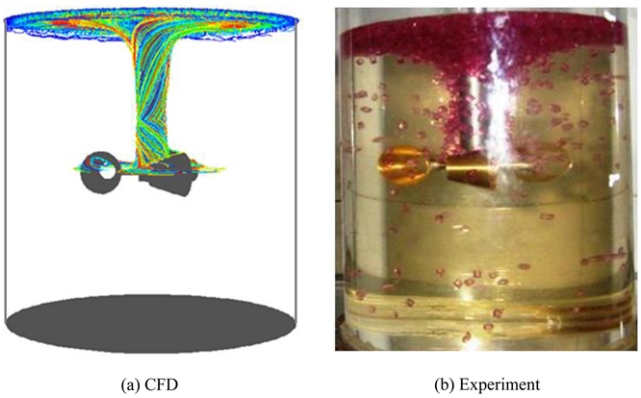

Fig. 7. Experimental and CFD results of particle spreading at the start of mixing.

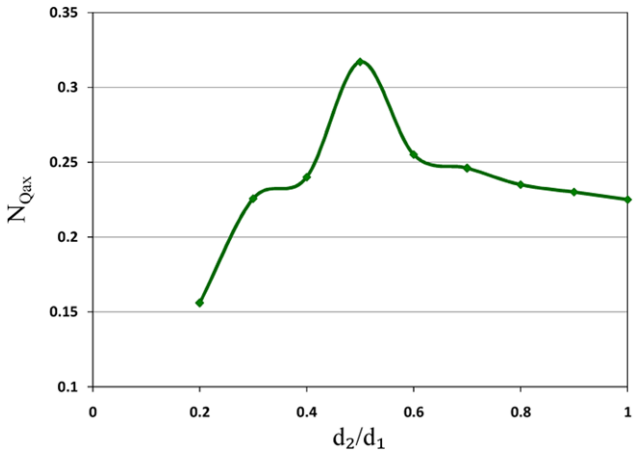

Fig. 8. Average axial flow number for different impeller geometries.

occurs inside the fluid. Both pictures show that regarding the established flow pattern inside the tank, the particles start to drawdown in a path close to the impeller shaft.

2. Hydrodynamics Characterization

In this part, the average axial flow number and average axial circulation time are calculated using the CFD predicted results. This was done in order to find the hydrodynamic characteristics of all examined impellers from a theoretical point of view.

In Fig. 8 the average axial flow numbers for all studied impellers are shown. The figure reveals that the impeller with diameter ratio of d_1/d_2=0.5 has the maximum value of the average axial flow number. Moreover, the predicted average axial circulation time, which is directly related to mixing time, is shown in Fig. 9. The figure reveals the lowest average axial circulation time for the impeller with diameter ratio of d_1/d_2=0.5. This was quite predictable from higher obtained average axial flow number for this impeller. By referring to these two figures, it is possible to explain the observed experimental results reported in section 2.

Finally, Figs. 10 and 11 illustrate the advantage of selected geometry, impeller with diameters ratio of d_1/d_2=0.5, in terms of power and energy consumption by different impellers. Turning to Fig. 10, the normalized difference in power consumption by each impeller

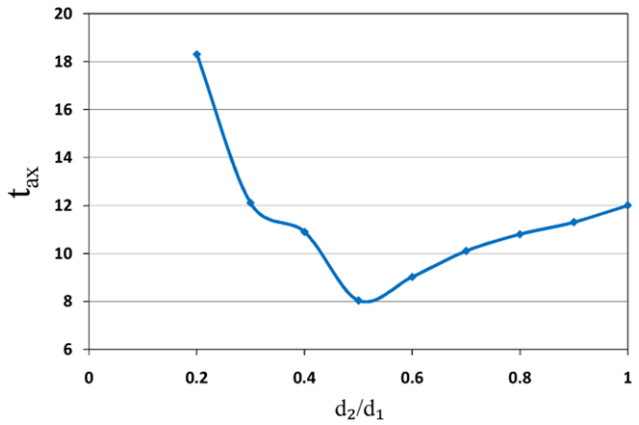

Fig. 9. Average axial circulation time for different impeller geometries.

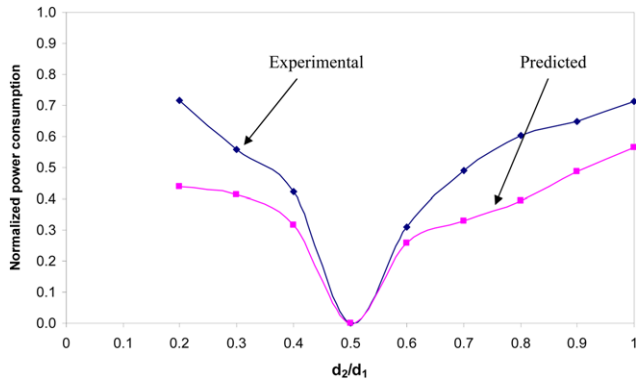

Fig. 10. Experimental and predicted normalized differences in power consumption by the impellers.

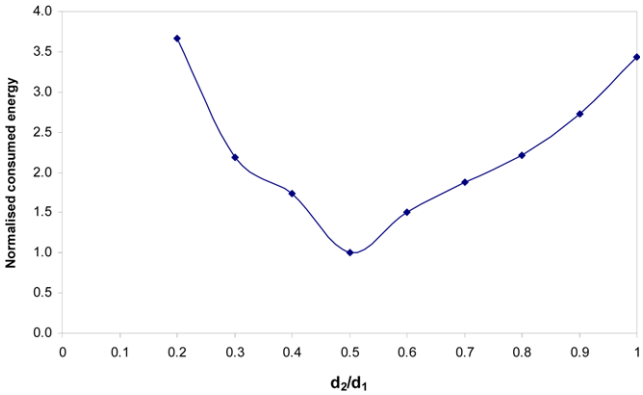

Fig. 11. Normalized predicted energy consumption by different impeller geometries.

which defined in Eq. is used as a comparison criterion.

$$\text{normalized difference in power consumption} = \frac{P - P_{eff}}{P}$$

In which P is power consumed by corresponding impeller and P_{eff} is power used by the efficient impeller, d_1/d_2=0.5.

The results reveal the same trend for both experimental and predicted normalized difference in power consumption. However, there are considerable differences in values, which can be explained by different electrical power lost in electrical electromotor for different impellers. The more difference is obtained for impellers with lower performance (d_1/d_2=0.2 and d_1/d_2=1.0), which confirms this explanation.

On the other hand, in Fig. 11 in order to evaluate an order for energy consumption by the studied impellers, the multiple of power consumption (using Eq. (13)) and average axial circulation of each impeller has been used as criterion. The result of this calculation, as normalized energy consumption, which is the ratio of energy consumed by each impeller to energy used by the efficient one, is presented in Fig. 10. The results show that the other impellers use at least 1.5 times energy compared with the efficient one and in some cases it reaches to more than 3.5 times. This confirms that the impeller with diameter ratio of d_1/d_2=0.5 works more efficiently in comparison with the other examined impellers. This result reveals that this optimum geometry of impeller could reduce the energy consumption even more than one-third of those obtained using the worst ones.

CONCLUSIONS

In the present work a study has been undertaken to find fluid flow characteristics of arecently developed impeller called Visco-jet. Regarding the semi-conical shape of this impeller's blades, experimental works were carried out to examine its performance at various diameter ratios of two sides of the blade. Based on this idea nine impellers with different impeller blade diameter ratios were fabricated and their performance in drawdown of some floated polymeric particles was examined. From measuredrotational speeds of $N_{JD(f)}$ and $N_{JD4\text{-}6}$ as well as power consumption by these impellers, it can be concluded that the shape of the semi-conical impeller's blades has a significant effect on the way of the particle drawdown inside the vessel. The impeller with two side diameters ratio of 0.5 showed the best performance among the studied impellers. Moreover, this geometry used the lowest power compared with those of the other one. From this observation it can be concluded that impellers with the highest and lowest diameter ratios do not work efficiently and cause a poor mixing performance.

In this research, the three-dimensional CFD modeling technique using DPM model of particles movement was employed to explain the experimental observation. Two groups of macroindicators, includingpower number, circulation number, impeller flow number, axial flow number and local indicators such as velocity profiles, streamlines and particles tracking, were used for this purpose. The results of this analysis confirm that the impeller's blade geometry has a significant effect on these hydrodynamic parametersand the impeller with two side diameter ratio of 0.5 works more efficiently compared with the other ones.

NOMENCLATURE

A : radial section of the tank [m^2]
C : torque [N·m]
C_d : drag coefficient
D : impeller diameter [m]
d : shaft diameter [m]
d_p : particle diameter
F_i : additional forces
$F_D(u_i - u_i^p)$: drag force per unit particle mass [m s^{-2}]
g_i : acceleration of gravity in the i-direction
H : liquid height in the tank [m]
K_p : power constant
N : impeller rotational speed [rpm]
N_{JD} : draw down speed
N_{js} : critical impeller speed
N_p : power number
$N_{Q_{Aax}}$: average axial flow number
$N_{Q_{ax}}(z)$: axial flow number
P : power consumption [W]
P_{eff} : power consumption by the efficient impeller [W]
Q_{Aax} : average axial flow rate [m^3 s^{-1}]
$Q_{Aax}(z)$: axial flow rate [m^3 s^{-1}]
Re : Reynolds number

T : vessel diameter [m]
t_{ax} : average axial circulation time [s]
V : liquid volume [m^3]
v : solid phase velocity
v_z : axial velocity [m s^{-1}]
u : velocity component
u : fluid phase velocity
u_i : Fluid velocity in the i-direction
u_i^p : particle velocity in the i-direction
Z : axial coordinate [m]

Greek Symbols

μ_f : viscosity of the fluid
ρ_f : fluid density [kg m^{-3}]
ρ_s : particle density [kg m^{-3}]
ε : bed voidage

Subscripts

JD : just draw down
JD(f) : just draw down (first)
JS : just suspended

Abbreviations

PBT : pitched blade turbine
LE-20 : proprietary impeller (by Hayward Tyler Ltd.)

REFERENCES

1. S. H. Kim, A. Bidkar, H. H. Ngo, S. Vigneswaran and H. Moon, *Korean J. Chem. Eng*., **18**, 163 (2001).
2. S. G. Kim, K. J. Choi, P. J. Yu, S. H. Kim and Y. D. Lee, *Korean J. Chem. Eng*., **25**, 19 (2008).
3. G. O. Taskin and H. Wei. *Chem. Eng. Sci*., **58**, 2011 (2003).
4. N. Kuzmanić and B. Ljubičić, *Chem. Eng. J*., **84**, 325 (2001).
5. A. Iranshahi, M. Heniche, F. Bertrand and P. A. Tanguy, *Chem. Eng. Sci.*, **61**, 2609 (2006).
6. A. Iranshahi, C. Devals, M. Heniche, L. Fradette, P. A. Tanguy and K. Takenaka, *Chem. Eng. Sci.*, **62**, 3641 (2007).
7. J. E. Pérez-Terrazas, V. Ibarra-Junquera and H. C. Rosu, *Korean J. Chem. Eng*., **25**, 461 (2008).
8. A. K. Sahu, P. Kumar, A. W. Patwardhan and J. B. Joshi, *Chem. Eng. Sci.*, **54**, 2285 (1999).
9. B. H. Um and T. R. Hanley, *Korean J. Chem. Eng.*, **25**, 1094 (2008).
10. L. Pakzad, E. Ein-Mozaffari and P. Chan, *Chem. Eng. Process*., **47**, 2218 (2008).
11. G. R. Kasata, A. R. Khopkar, V. V. Ranadeb and A. B. Pandita, *Chem. Eng. Sci.*, **63**, 3877 (2008).
12. H. Yamazaki, K. Tojo and K. Miyanami, *Powder Technol*., **48**, 205 (1986).
13. F. Barailler, M. Heniche and P. A. Tanguy, *Chem. Eng. Sci.*, **61**, 2888 (2006).
14. G. O. Taskin, *Chem. Eng. Sci.*, **61**, 2871 (2006).
15. A. P. Van der Westhuizen and D. A. Deglon, *Mineral. Eng.*, **20**, 233 (2007).
16. FLUENT 6.2 ®, FLUENT Inc., Lebanon, NH, USA (2005).
17. H. K. Versteeg and W. Malalasekera, *An introduction to computational fluid dynamics: The finite volume method*, first Ed., Longman Limited, England (1995).
18. T. B. Anderson and R. Jackson, *Computational fluid dynamics: The basic with applocation*, McGraw-Hill. Inc. (1995).
19. R. B. Bird, W. E. Stewart and E. N. Lightfoot, Transport Phenomena, John Wiley & Sons, Inc. (2002).
20. M. Alliet-Gaubert, R. Sardeing, C. Xuereb, P. Hobbes, B. Letellier and P. Swaels, *Chem. Eng. Process*., **45**, 415 (2006).